Dilatancy, brittle strength, and anisotropy of foliated rocks: Experimental deformation and micromechanical modeling

Geoffrey C. Rawling,[1] Patrick Baud,[2] and Teng-fong Wong
Department of Geosciences, State University of New York at Stony Brook, Stony Brook, New York, USA

Received 14 February 2001; revised 7 April 2002; accepted 12 April 2002; published 17 October 2002.

[1] Triaxial compression experiments were performed on the Four-mile gneiss. The biotite foliation in the Four-mile gneiss results in dilatancy and strength anisotropies, which become more pronounced with increasing confining pressure. Microstructural observations indicate that when there is high resolved shear stress on the macroscopic foliation, dilatancy arises from extensile microcracks nucleated by frictional slip on biotite grains. Evolution of crack geometry and coalescence are also influenced by the biotite foliation. Motivated by these observations, a damage mechanics model based on sliding wing cracks was adopted to analyze the anisotropic development of dilatancy and brittle fracture. Frictional coefficients for the sliding cracks are inferred to be comparable to those of cleavage surfaces of biotite. The strength anisotropy data of the Four-mile gneiss can be explained by the variation of the initial damage with the foliation angle. The damage derives from a set of preexisting microcracks with random orientation, and a set of cleavage cracks in mica grains preferentially oriented along the foliation angle. Hence, the initial damage is higher for the intermediate angles, and, consequently, the strength is somewhat lower. The observation that the mechanical strengths of a variety of foliated rocks decrease with increasing mica content can be explained by the same model, with the implication that the initial damage and mica content are linearly related. The mechanical and microstructural data show that dilatancy anisotropy may significantly influence the progressive development of borehole breakout and strain localization. *INDEX TERMS:* 5104 Physical Properties of Rocks: Fracture and flow; 5112 Physical Properties of Rocks: Microstructure; 7207 Seismology: Core and mantle; *KEYWORDS:* dilatancy, anisotropy, mica, cracks, damage mechanics

Citation: Rawling, G. C., P. Baud, and T.-f. Wong, Dilatancy, brittle strength, and anisotropy of foliated rocks: Experimental deformation and micromechanical modeling, *J. Geophys. Res.*, *107*(B10), 2234, doi:10.1029/2001JB000472, 2002.

1. Introduction

[2] The phenomenon of mechanical anisotropy has received considerable interest in rock physics and structural geology. Bedding in sedimentary rocks, cleavage in slates, and preferred orientation and/or arrangement of minerals and cracks in crystalline igneous and metamorphic rocks are some examples of planar anisotropic rock fabrics that lead to mechanical anisotropy. Elastic anisotropy of a rock can be related to its fabric, a seismic manifestation of which is shear wave splitting [e.g., *Brace*, 1965; *Barroul and Mainprice*, 1993; *Siegesmund et al.*, 1993]. Textural anisotropy can also result in significant anisotropy of tensile [*Nova and Zaninetti*, 1990; *Liao et al.*, 1997] and compressive [e.g., *Donath*, 1964; *Borg and Handin*, 1966; *Vernik et al.*, 1992a; *Shea and Kronenberg*, 1993] strength, that may be associated with different failure modes and deformation mechanisms, depending on how stress is applied relative to the anisotropy planes. Illustrative examples were provided by *Donath* [1964] on slate, *Paterson and Weiss* [1966] on phyllite, and *Kronenberg et al.* [1990] on single crystals of biotite. These studies have also documented the transition of compressive failure mode from kinking, to frictional or plastic slip, to brittle faulting as the angle between the plane of weakness and the compression axis increases.

[3] One of the objectives of this work is to address the interrelationships of textural anisotropy, dilatancy, and the micromechanics of compressive failure. Dilatancy, defined as inelastic volume increase, is universally observed as a precursor to the inception of shear localization in the brittle faulting regime [*Brace et al.*, 1966; *Paterson*, 1978]. The onset and development of dilatancy are often associated with acoustic emission (AE) activity, and it can be traced to the nucleation and growth of stress-induced cracks that are subparallel to the maximum compressive stress [*Tapponier and Brace*, 1976]. These cracks eventually grow to a length comparable to their spacing and interact with one another, leading to macroscopic fault formation and failure [*Wong*, 1982; *Kranz*, 1983]. It is recognized that the microcracks nucleate from tensile stress concentrations, which may arise from frictional sliding along inclined cracks or grain boun-

[1]Now at New Mexico Bureau of Geology and Mineral Resources, Socorro, New Mexico, USA.
[2]Now at Institut de Physique du Globe, Université de Louis Pasteur, Strasbourg, France.

0148-0227/02/2001JB000472$09.00

daries, crystal plasticity (e.g., twinning), or shear deformation of weak phases (such as mica) [*Brace et al.*, 1966; *Tapponier and Brace*, 1976; *Kranz*, 1979; *Fredrich et al.*, 1989].

[4] Previous studies of dilatancy and micromechanics of failure have focused on relatively isotropic rocks. To our knowledge, the onset and development of dilatancy in foliated rocks have not been systematically investigated. Notwithstanding the paucity of laboratory data, assumption of dilatancy anisotropy has been (implicitly or explicitly) incorporated into the interpretation of borehole breakouts and in situ stress measurements [e.g., *Vernik et al.*, 1992b]. It may also play a significant role in the localization of strain in retrograde shear zones [e.g., *Gibson*, 1990].

[5] Our experimental deformation focuses on the Four-mile gneiss, the strength anisotropy of which was previously investigated by *Gottschalk et al.* [1990]. They defined a three-dimensional failure envelope with orthorhombic characteristics that is related to the symmetry of the foliation and lineation of biotite within the rock. In this study we investigated the anisotropic mechanical behavior of the Four-mile gneiss by conducting triaxial compression experiments with volumetric strain and AE measurements, as well as detailed microstructural observations that have yielded new insight into the micromechanics of dilatancy and damage evolution in this foliated rock. Two related questions are addressed in this study. Is the critical stress for the onset of dilatancy anisotropic? If so, why and how is it related to the peak stress anisotropy?

[6] Traditionally the effect of textural anisotropy on compressive strength has been analyzed by incorporating a ''plane of weakness'' into the empirical Coulomb criterion [*Jaeger and Cook*, 1979] or modified Griffith criterion [*Walsh and Brace*, 1964]. More refined models have been proposed [e.g., *Horii and Nemat-Nasser*, 1986; *Kemeny and Cook*, 1987; *Ashby and Sammis*, 1990] for the progressive development of dilatancy and compressive failure in rock. While such damage mechanics models basically capture the micromechanics of the nucleation, propagation and coalescence of stress-induced microcracks, they have been applied only to relatively isotropic rocks. In this study, we adapted the damage mechanics model of *Ashby and Sammis* [1990] to analyze the observed mechanical anisotropy in terms of crack nucleation around a preexisting weak phase and the influence of the preferred orientation of biotite on subsequent damage accumulation. Synthesis of our mechanical data and those of *Shea and Kronenberg* [1993] indicates an overall trend for the brittle strength of a foliated rock to decrease with increasing mica content. The damage mechanics model was also used to interpret this weakening trend in terms of the connection between initial damage state and mica content. The implications of our results for related tectonic and geophysical processes will also be discussed.

2. Mechanical Deformation

2.1. Sample Material and Preparation

[7] A detailed petrographic description and analysis of the Four-mile gneiss were given by *Gottschalk et al.* [1990]. The modal composition of the rock is: 46.1% plagioclase, 29.0% quartz, 14.8% microcline, 9.0% biotite and 1.0% muscovite. Plagioclase grains have lengths ranging from 0.1 to 2.8 mm. Quartz and microcline grains are subequant, with effective diameters in the ranges 0.05–1.6 mm and 0.1–1.1 mm, respectively. Biotite, the predominant phyllosilicate, occurs as isolated grains, 0.1–2.2 mm in length, and it defines a strong foliation and a lineation within the foliation. Measured poles to biotite grains define a strong maxima perpendicular to the macroscopic foliation. Petrographically our undeformed samples are indistinguishable from those in the previous study.

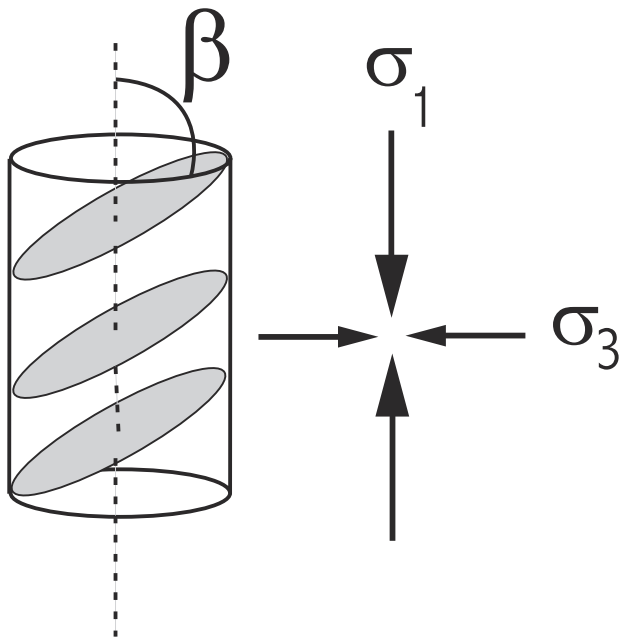

Figure 1. Reference scheme for sample orientation. β is the angle between the foliation plane and compression axis.

[8] The oriented samples for triaxial compression experiments were right circular cylinders, 38.1 mm in height and 18.4 mm in diameter, cored from a block collected from the same quarry as the starting material of *Gottschalk et al.* [1990]. The samples were cored in five orientations within a plane perpendicular to the macroscopic foliation and containing the lineation (corresponding to the x–z plane defined by *Gottschalk et al.* [1990]). Sample orientations are described by the angle β that specimen axis makes with the foliation (Figure 1).

[9] The sample was first dried in vacuum and weighed (ω_d), then saturated with distilled water and weighed again (ω_w), and the (interconnected) porosity is then given by $\phi = (\omega_w - \omega_d)/(\rho_w V)$, where ρ_w is the density of water and V is the sample volume. The porosities so measured for four randomly selected samples ranged from 0.5 to 0.9%. Hydrostatic compression data indicate that the crack porosity ranges from 0.2 to 0.3%, which requires a confining pressure of ~300 MPa for closure.

[10] The vacuum-dried samples were jacketed in thin copper foil (thickness 0.05 mm) and first pressurized to 200 MPa to seat the jacket and collapse it tightly onto the sample. One axial and one radial strain gauge (of lengths 10 mm and 13 mm, respectively) were then applied with epoxy to the jacketed sample surface. The samples were further jacketed in heat-shrink (polyolefine) tubing which was

Table 1. Mechanical Data of Four-Mile Gneiss

Foliation Angle β	Confining Pressure P_c, MPa	Young's Modulus E, MPa	Peak Stress, MPa	Dilatancy Onset Stress C', MPa	Yield Stress σ_y, MPa
0°	50	667	550	125	230
30°	50	530	392	50	110
45°	50	576	355	75	60
45°	50	588	[a]	75	130
60°	50	533	390	75	150
90°	50	558	512	100	88
45°	100		517	150	200
45°	150		645	108	180
0°	200	758	1060	345	320
0°	200	789	[a]	330	350
30°	200	722	762	472	200
30°	200	759	870	175	200
40°	200	689	737	112	115
45°	200	714	[a]	180	200
45°	200		[a]	180	200
60°	200		775	275	170
60°	200	659	765	190	120
90°	200	667	1010	200	200
90°	200	694	[a]	200	200
0°	300	879	1440	390	350
30°	300	784	875	230	200
45°	300	723	950	260	310
60°	300	727	1040	270	255
90°	300	762	1340	400	300

[a] Samples were unloaded near the peak stress for microstructural observations.

clamped to the steel end spacers with wire. Strain gauge leads were routed through holes in the tubing and sealed with silicone sealer. A piezoelectric transducer (PZT-7, 5.0 mm diameter, 1 MHz longitudinal resonant frequency) was attached to one spacer to monitor AE activity during the experiments.

2.2. Experimental Procedure

[11] We deformed 22 samples (with $\beta = 0°$, 30°, 45°, 60°, and 90°) in the conventional triaxial configuration at confining pressures (P_c) of 50, 200, and 300 MPa (Table 1). Two additional tests were performed on samples (with $\beta = 45°$) at $P_c = 100$ and 150 MPa. The confining pressure was monitored with a strain gauge pressure transducer with an accuracy of 0.5 MPa. The displacement rate was servo-controlled and fixed at 1 μm s^{-1}, corresponding to a nominal strain rate of 2.6×10^{-5} s^{-1}. The axial displacement was monitored with a displacement transducer between the ram and the fixed pressure vessel. The axial load was measured with an external load cell accurate to 1 kN. The volumetric strain was calculated using the relation $\varepsilon_{vol} = \varepsilon_{ax} + 2\varepsilon_{rad}$, where ε_{ax} and ε_{rad} are the strains measured in the axial and transverse directions, respectively. The strain measurements have an accuracy of 0.01%, estimated from drift during hydrostatic experiments. The AE signals were conditioned by a preamplifier and the characteristics of the signal were screened with a discriminator [see *Wong et al.*, 1997].

[12] Six samples were deformed at $P_c = 200$ MPa for microstructural observation. Three samples (FMG1, FMG5 and FMG6) at $\beta = 0°$, 45°, and 90°, respectively, were deformed to near the peak stress, as determined in previous experiments that ended in brittle failure, and then unloaded. Three experiments (FMG2, FMG3 and FMG4) were performed at $\beta = 45°$ to different stages of deformation between the onset of dilatancy and peak stress. The deformed samples were cut in half along the cylinder axis in a plane perpendicular to the foliation. One half was made into a standard optical thin section and the other was made into a thick (100 μm) crack section and ion-milled to remove surface-damage. Observations of the crack sections were made using a JEOL 5300 scanning electron microscope (SEM) with an accelerating voltage of 30 kV in back-scattered electron mode.

2.3. Mechanical Data

[13] All samples in triaxial compression tests failed by the formation of a single throughgoing fault. After attaining a peak stress, each of the samples underwent an unstable stress drop, except for the 45° sample at 300 MPa (which had a small, stable stress drop and the experiment was stopped at an axial strain of 2.5%). The fault orientations were at ~30° to the sample axis.

[14] Volumetric strain and AE measurements provide important information on the evolution of the failure process. A representative set of stress–strain–AE data (at $\beta = 0°$, $P_c = 200$ MPa) is presented in Figure 2. The axial, transverse and volumetric strains are plotted as functions of the differential stress, and cumulative AE counts are plotted against the axial strain. In this paper, compressive stresses and strains are considered to be positive. The onset of dilatancy (C') is marked by the stress level at which the differential stress–volumetric strain curve deviates from linearity [*Brace et al.*, 1966; *Hadley*, 1973], and the yield point (σ_y) is defined here to be the stress level at which the differential stress–axial strain curve deviates from linearity (Figure 2). Preexisting cracks are not fully closed until the application of 200–300 MPa confining pressure. Since tests performed at $P_c < 300$ MPa have a small initial nonlinear portion in the differential stress–strain curves corresponding to the closing of these cracks under differential stress, the reference lines for C' and σ_y were not fitted to these initial nonlinear regions (Figure 2). Our methodology for picking C' closely follows that described by *Hadley* [1973].

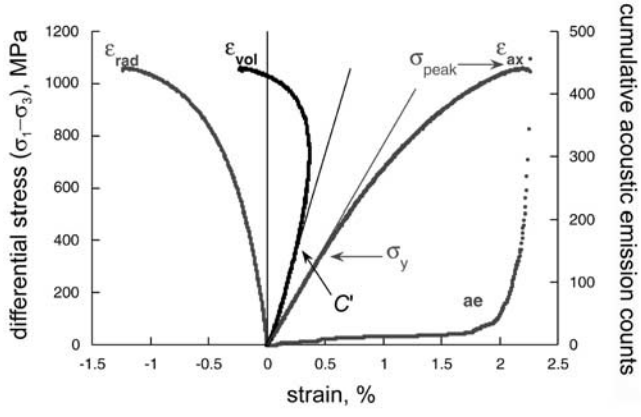

Figure 2. Representative stress–strain curves and acoustic emission data (for $\beta = 0°$ at confining pressure of 200 MPa). The axial, radial, and (calculated) volumetric strain data are shown. The yield stress and onset of dilatancy are also marked.

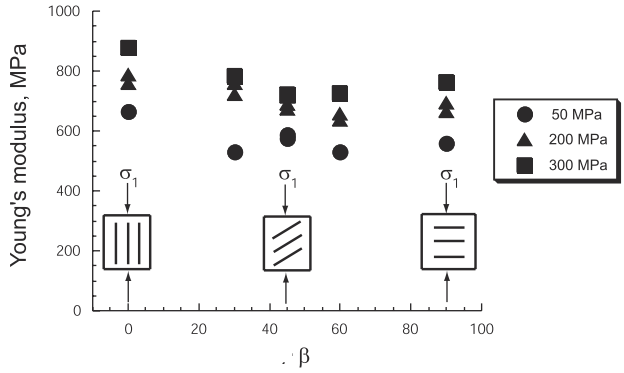

Figure 3. Young's modulus as function of foliation angle β and confining pressure.

[15] The AE activity typically surged at ~90% of the peak stresses in all tests. The general form of the stress–strain curves and AE activity are similar at all β values. Mechanical data from the triaxial tests are compiled in Table 1. There is no systematic trend for the amount of dilatancy before failure to vary with β. However, there is a general decrease in the amount of dilatancy with increasing pressure.

[16] The slope of the elastic reference line for σ_y determination (Figure 2) corresponds to Young's modulus in the axial direction. It is plotted as a function of β for P_c = 50, 200 and 300 MPa in Figure 3. For fixed β, Young's modulus increases with increasing P_c. This increase is due to the elastic closure of microcracks. There is an overall decrease of Young's modulus with increasing β that levels off at higher angles, in agreement with theoretical predictions [*Amadei*, 1983; *Tien and Tsao*, 2000]. Biotite is most compressible parallel to [001] [*Simmons and Wang*, 1971], and thus, all other mineral orientations being random, the rock should be most compressible when β = 90°. This trend is clearest at P_c = 300 MPa because at lower pressures the open cracks obscure this foliation effect on Young's modulus.

[17] Figures 4a and 4b show the onset of dilatancy C' and peak stress as functions of P_c and β. There is appreciable sample-to-sample variability. This is not unexpected since some ambiguity is involved in picking C': *Hadley*'s [1973] data for a large number of samples indicate that the variation in C' from sample to sample at any one confining pressure may be as much as 100 MPa for Westerly granite and twice that for the San Marcos gabbro. To our knowledge, this is the first comprehensive set of data on the concomitant variation of C' and brittle strength as functions of foliation orientation and confining pressure. The onset of dilatancy and peak stresses follow qualitatively similar trends in anisotropy. While there is no resolvable anisotropy in peak stress or C' at P_c = 50 MPa, it is considerable at P_c = 300 MPa. The peak differential stresses and their variation with β agree with the results of *Gottschalk et al.* [1990]. The general trend of a minimum in the peak stress at β = 30–45° and maxima at β = 0° and 90° is typical of texturally anisotropic rocks such as shale [*Niandou et al.*, 1997], sandstone [*McLamore and Gray*, 1967], slate, phyllite, and schist [*Donath*, 1972] and gneiss and amphibolite [*Vernik et al.*, 1992a].

3. Microstructural Observations of Deformed Samples

[18] In general the deformation microstructure in the gneiss is similar to granite and other low-porosity crystalline rocks deformed in the brittle field [*Tapponier and Brace*, 1976; *Wong*, 1982; *Kranz*, 1983; *Wong and Biegel*, 1985; *Hirth and Tullis*, 1989; *Chang and Haimson*, 2000]. All samples failed along macroscopic faults formed by the growth and coalescence of extensile microcracks with a predominant orientation parallel to the maximum compressive stress. The optical microscopy observations of *Gottschalk et al.* [1990] on failed samples apply equally well in this study. However, our SEM and optical microscopy observations on samples at different stages of deformation provide new insight into the damage evolution process, especially crack nucleation and propagation around biotite grains and the effect of the biotite on the subsequent crack coalescence.

3.1. β = 45°: Nucleation and Propagation of Stress-Induced Cracks

[19] Sample FMG2 was deformed to just beyond the onset of dilatancy C'. The most significant observation in this sample is that there is evidence for crack growth around biotite grains oriented favorably for frictional slip on cleavage. Figure 5a shows cracks subparallel to the com-

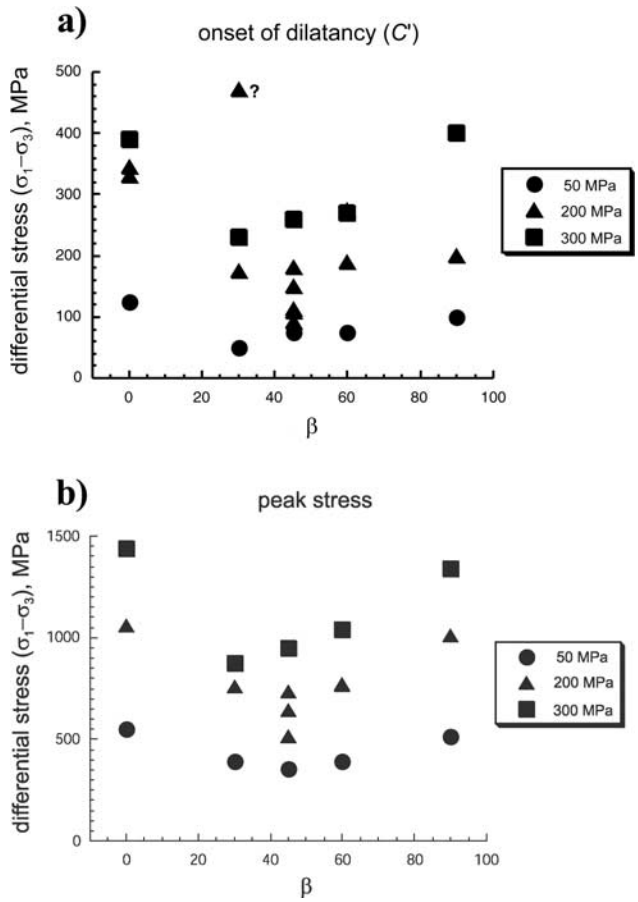

Figure 4. (a) Stress for the onset of dilatancy as function of foliation angle β and confining pressure. (b) Peak stress as function of foliation angle β and confining pressure.

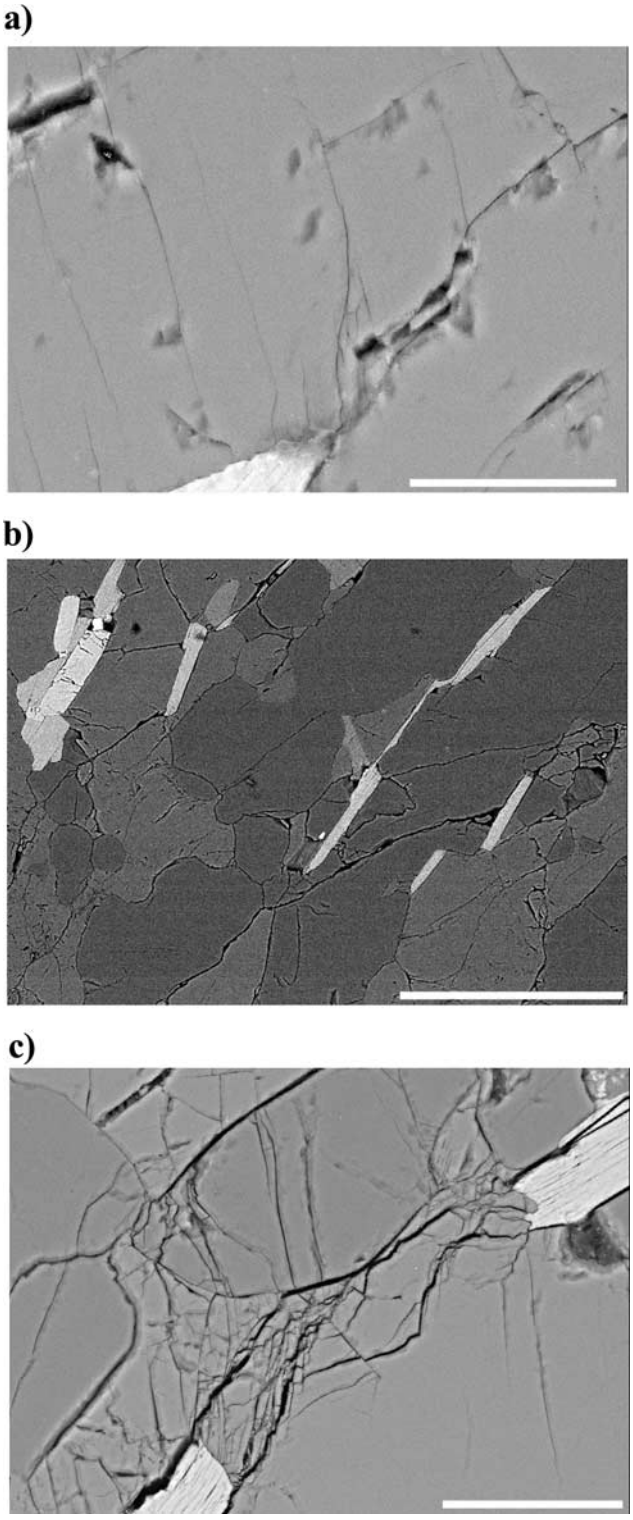

Figure 5. (a) SEM image of FMG2 showing nucleation of wing cracks from the tip of a biotite grain (lighter area at lower part of micrograph). Direction of σ_1 was vertical, and scale bar is 50 μm. (b) SEM image of FMG4 showing incipient linkage of cracks. Note the grain boundaries are mostly cracked. Direction of σ_1 was vertical, and scale bar is 200 μm. (c) SEM image of FMG5 showing crack coalescence and brecciation between adjacent biotite grains. Arrays of subvertical cracks are also present. Direction of σ_1 was vertical, and scale bar is 100 μm.

pression axis nucleating at a biotite grain. These are typical of stress-induced microcracks [*Tapponier and Brace*, 1976; *Kranz*, 1983], with very low aperture-to-length ratios, smooth, parallel sides, essentially constant width, and very sharp terminations, often within grains. The biotite grain has probably undergone sliding on an open cleavage crack, but slip displacements along such sliding cracks are difficult to resolve even under the SEM [*Wong*, 1982; *Wong and Biegel*, 1985]. Shear deformation in the biotite would cause a stress concentration at the end of the grain, which was relieved by the formation of tensile cracks. Such a scenario would be most favored at $\beta = 30°$ and 45°, resulting in an earlier onset of dilatancy at these orientations.

[20] At greater strains, crack growth continued to be most intense around biotite grains oriented favorably for shear. Sample FMG4 was deformed to the stage at which a surge in AE activity indicated the imminent attainment of the peak stress. This sample shows intense zones of cracking around the tips of the grains (Figure 5b). Most of the grain boundaries are cracked. At this stress, kinking has begun in some of the biotite grains. Crack coalescence is more intense in sample FMG5 which was deformed to near the peak stress. Figure 5c shows a ''brecciated'' zone in this sample that has linked two biotite grains.

3.2. $\beta = 0°, 90°$: Effect of Foliation on Crack Propagation and Arrest

[21] For orientations $\beta = 0°$ and 90°, biotite is not oriented favorably for slip and typically deforms by kinking and faulting, respectively. (See *Kroanenberg et al.* [1990] for results on single crystals). Sample FMG1 ($\beta = 0°$) was deformed to near the peak stress. Figure 6a shows some of the complex kink geometries that develop in biotite grains oriented at low angles to the compression axis. Note especially the formation of voids and the tendency for the kink boundaries to trend diagonally across the basal planes. Sample FMG6 ($\beta = 90°$) was deformed to near the peak stress. Intense intragranular cracking in feldspar and quartz grains which probably resulted from elastic mismatch between the compliant biotite and the stiff feldspar or quartz in between can be seen. The elongate biotite grains often seem to act as barriers for the linkage of cracks across more than one grain (Figure 6b).

3.3. Crack Coalescence

[22] The three samples loaded to near the peak stresses were examined under the petrographic microscope to characterize the geometry of crack coalescence. Photomicrograph mosaics of cracks arrays at (10x magnification) of FMG1, FMG5, and FMG6 are shown in Figures 7a, 7b, and 7c, respectively. The biotite grains appear to exert some degree of control on the geometry of the growing crack arrays. This is most evident in comparison of $\beta = 45°$ and 90° (Figures 7b and 7c). At $\beta = 45°$ the cracks between biotite grains are localized in narrow zones that link the ends of grains. The upper left of Figure 7b is typical. Grain boundary cracks appear to be more common than intragranular cracks. This may be due to the weak shape preferred orientation of the other minerals in the Four-mile gneiss. Quartz often occurs as subequant grains arranged in zones subparallel to the foliation, and as a result, the foliation planes tend to have a higher concentration of grain

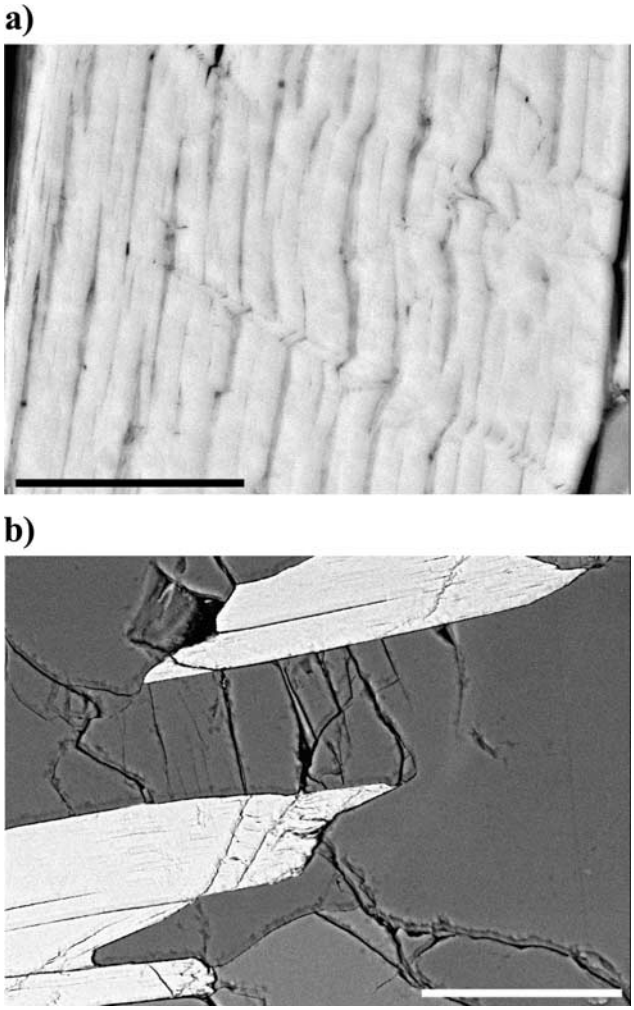

Figure 6. (a) SEM image of a single biotite grain from FMG1 showing development of kink bands. Note the complex geometry and inclination of kink bands relative to basal planes of the biotite. Direction of σ_1 was vertical, and scale bar is 25 μm. (b) SEM image of FMG6 showing crack coalescence in an incipient fault. Direction of σ_1 was vertical, and scale bar is 150 μm.

boundaries. At $\beta = 90°$, the cracked zones are much wider, with extensive cracking visible even around localized brecciated zones as in the bottom portion of Figure 7c. As at $\beta = 45°$, biotite grains localize deformation, but their orientations are unfavorable for the transfer of macroscopic slip and thus act as barriers to the development of shear localization. To overcome such barriers and attain the critical damage geometry for the inception of shear localization, the crack arrays between biotites are wider and have much more intense intragranular cracking (e.g., the top of Figure 7c; many feldspar cleavage cracks are visible).

[23] At $\beta = 0°$ (Figure 7a), the cracks linking biotite grains are similar to those at $\beta = 90°$. Intragranular cracks are more common than at $\beta = 45°$ but not as common as at $\beta = 90°$, and some arrays emanating from biotite grains are very localized, as in the top of Figure 7a. To the right of the figure, some very long grain boundary cracks are present. This is consistent with the weak preferred grain boundary orientation being parallel to the maximum compressive stress.

3.4. Failure Mode of Biotite

[24] Previous studies have underscored the important role that crystal plastic processes in biotite play in triggering and controlling microcracking and shear localization in isotropic [*Tapponier and Brace*, 1976; *Wong and Biegel*, 1985; *Chang and Haimson*, 2000] and anisotropic [*Gottschalk et al.*, 1990; *Shea and Kronenberg*, 1993] rocks. While our observations are in general agreement with previous work, we have noted several new and important features.

[25] To our knowledge, we have obtained some of the first observations of shear-induced wing cracks in samples that have undergone dilatancy (Figure 5a). In the relatively isotropic Westerly granite, *Tapponier and Brace* [1976] only observed the opening of grain boundaries and healed cracks in samples deformed to just beyond C'. The absence of shear-related wing cracks is often cited as evidence against the use of a class of theoretical models (formulated by *Horii and Nemat-Nasser* [1986], *Ashby and Hallam* [1986], and *Kemeny and Cook* [1987]) for the onset and development of dilatancy in brittle rock. While shear-induced wing cracks were inferred to have propagated and coalesced in failed samples of anisotropic rock similar to the Four-mile gneiss [*Gottschalk et al.*, 1990; *Vernik et al.*, 1992a, 1992b; *Shea and Kronenberg*, 1993], the microstructure of samples deformed to well beyond C' does not provide much information on the nucleation and propagation processes. Our observations of wing crack nucleation due to shear deformation in biotite grains at $\beta = 45°$ (and by inference at $\beta = 30°$ and $60°$) provide microstructural basis for the damage mechanics model to be formulated in the next section.

[26] Biotite grains are commonly considered to act as nuclei that promote the development of crack coalescence and macroscopic fracture [*Tapponier and Brace*, 1976; *Wong and Biegel*, 1985; *Gottschalk et al.*, 1990]. Our observations show that this is not universally true for all orientations in anisotropic rock. In particular, the biotite grains act more as barriers for crack propagation when the foliation is oriented at high angles to the compression axis, even though they may be a source of elastic mismatch cracks (Figures 6b and 7c).

[27] In light of this "dual" role of biotite deformation in the micromechanics of failure, we characterized quantitatively the intensity of kinking in biotite as a function of β. Kink orientations were measured optically in traverses across thin sections of FMG1, FMG3, FMG4, and FMG5. In each thin section, 100 biotite grains were observed in a traverse across the central portion of the thin section and the orientations of kink bands relative to the compression axis were measured. The details of the kinks are not resolvable in normal thin sections even at high magnification, but the orientations of the kink bands can be measured. No kinks were observed in FMG2 and less than 1% of the biotite grains in FMG 6 are kinked.

[28] In Figures 8a and 8b the kink orientation data from FMG1 and FMG3, FMG4, and FMG5 combined are plotted against kink boundary angle. More than 90% of the biotite grains in FMG1 are kinked. There is a preferred orientation at 66° from the compression axis. This is consistent with the majority having formed in response to the remote applied

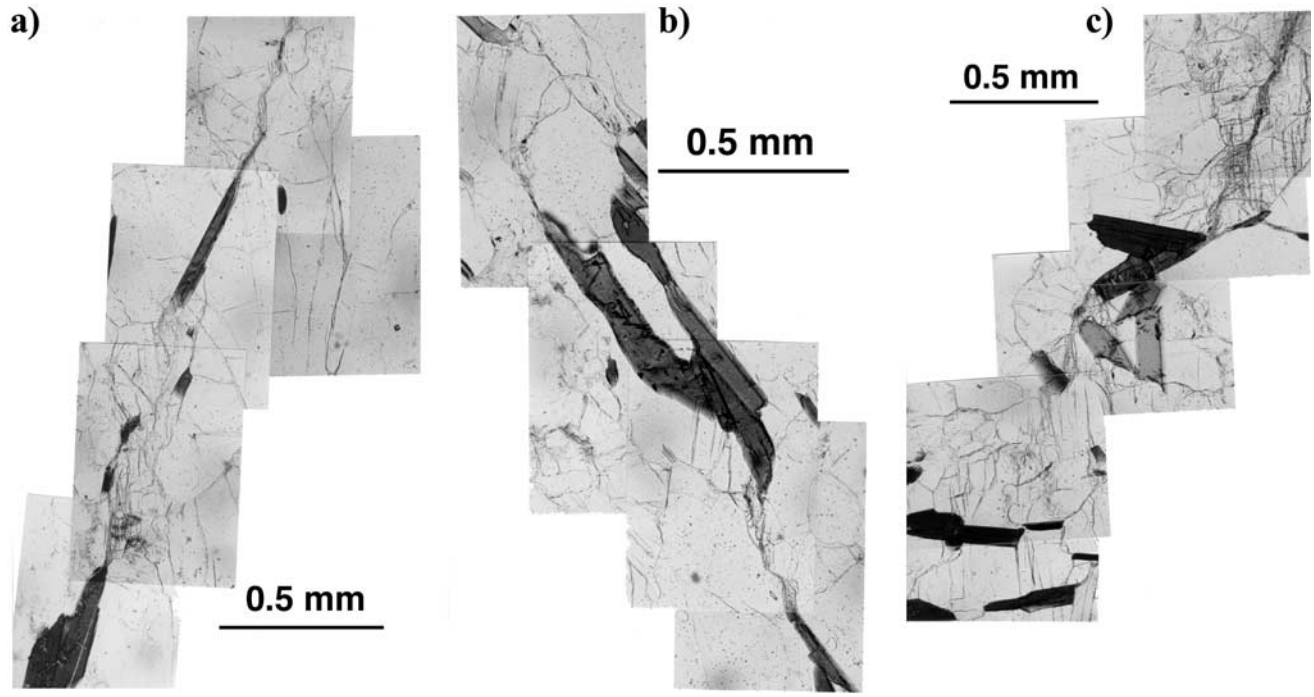

Figure 7. (a) Optical micrograph mosaic of sample FMG1 showing coalescence of kinked biotite grain and crack arrays. Direction of σ_1 was vertical. (b) Optical micrograph mosaic of sample FMG5 showing coalescence of cleavage cracks in biotite and wing cracks. Direction of σ_1 was vertical. (c) Optical micrograph mosaic of sample FMG6 showing coalescence of subvertical crack arrays and biotite grains acting as barriers to the development of shear localization. Direction of σ_1 was vertical.

stress field, since the orientations of kinks are similar to what has been observed in experimental studies on slate [*Gay and Weiss*, 1974] and phyllite [*Paterson and Weiss*, 1966] in which samples were compressed parallel to the foliation. In FMG5, 21% of the biotite grains are kinked. There are a wide range of orientations, with slightly preferred orientations at 30° and 60°, and a minimum at 45°. This suggests they are mostly a response to local stress perturbations, possibly due to basal slip.

4. Damage Mechanics of Dilatancy and Brittle Failure in Foliated Rocks

[29] Many empirical relations have been advanced to describe the orientation dependence of strength in anisotropic rocks [e.g., *McLamore and Gray*, 1967; *Donath*, 1972; *Gottschalk et al.*,1990]. In addition several theoretical models have been proposed. *Jaeger* [1960] described the single plane of weakness and continuously varying shear strength theories, which involve the variation with direction of the cohesive strength and internal friction parameters of the Mohr–Coulomb failure criterion. However, *Donath* [1972] emphasized that these parameters have no physical meaning in terms of fundamental rock properties. *Walsh and Brace*'s [1964] modified Griffith criterion yields similar predictions but is based on the orientations and friction coefficients of preexisting crack populations and thus is easily linked to rock properties. Yet these models are strictly only criteria for the activation of slip on a critically oriented "plane of weakness" or crack and thus do not predict the failure stress, because, as was first noted by *Brace and Bombolakis* [1963], fracture of brittle materials involves both the nucleation of cracks and their subsequent growth and coalescence to form a macroscopic fault.

[30] The more recent fracture mechanics formulations attempt to quantify both of these aspects of failure. The microstructural observations suggest that slip on favorably oriented biotite grains leads to crack nucleation that results in macroscopic dilatancy (Figure 5a). In many aspects, this scenario is captured by the "sliding wing crack" model [*Brace et al.*, 1966; *Horii and Nemat-Nasser*, 1986; *Ashby and Hallam*, 1986; *Kemeny and Cook*, 1987]. If the resolved shear stress on an inclined crack, which may be identified as a cleavage crack in a biotite grain, exceeds the frictional strength, slip occurs and tensile stress concentration develops at the tips of the inclined sliding crack (Figure 9). Extensile wing cracks nucleate and propagate along a direction subparallel to σ_1, the maximum principal stress. The initial propagation of a wing crack is stable, in that stress must be continuously increased for it to extend, but the mutual interaction of the stress fields of multiple wing cracks may lead to instability, which corresponds to the onset of shear localization and macroscopic fracture [*Horii and Nemat-Nasser*, 1986; *Sammis and Ashby*, 1986; *Kemeny and Cook*, 1987].

4.1. Onset of Dilatancy: Isotropic and Anisotropic Nucleation Conditions

[31] Consider a crack of length 2a inclined at an arbitrary angle γ to σ_1 (Figure 9). When frictional slip occurs on this inclined crack, the stress concentrations at its tips may induce "wing cracks" to nucleate at an angle of 70.5° to

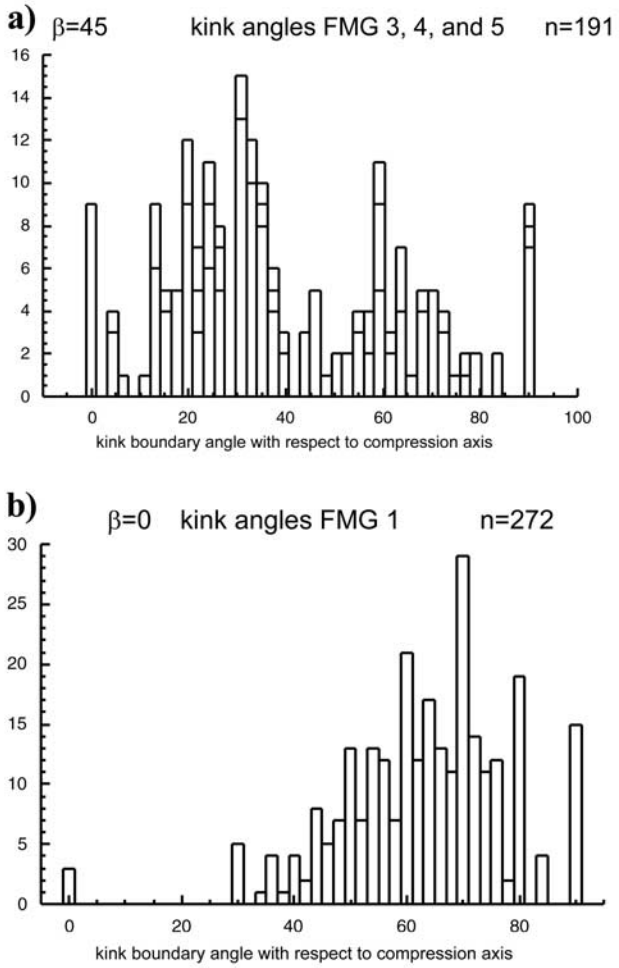

Figure 8. Orientations of kink bands in mica grains at two foliation orientations measured in optical thin sections of deformed samples. (a) Data of FMG3, 4, and 5 that show no preferred orientation for kink bands. (b) Data of FMG1 that show a preferred orientation at ~66° from the direction of σ_1.

the sliding crack. As summarized by *Ashby and Sammis* [1990], assuming that the inclined cracks are randomly oriented, then the wing cracks will first nucleate from sliding cracks critically oriented at $\gamma = 1/2 \tan^{-1}(1/\mu)$ when the principal stresses are related by:

$$\sigma_1 = m\sigma_3 + c \tag{1}$$

with,

$$m = \frac{\sqrt{1+\mu^2}+\mu}{\sqrt{1+\mu^2}-\mu}, \tag{2a}$$

and

$$c = \frac{\sqrt{3}}{\sqrt{1+\mu^2}-\mu}\frac{K_{1C}}{\sqrt{\pi a}}. \tag{2b}$$

In this formulation, it is implicitly assumed that μ (the coefficient of friction of the inclined sliding crack) and K_{1C} (the tensile fracture toughness of the material through which the wing crack propagates) are relatively uniform throughout the rock, with negligible variability among different minerals and crystal orientations. We will refer to this end-member scenario as "isotropic nucleation".

[32] Because biotite has a relatively low frictional coefficient [*Horn and Deere*, 1962], frictional slip will be activated first in biotite if favorably oriented cleavages are available. However, in the biotite grains the potential sliding surfaces will not be randomly oriented. A majority will have orientations close to $\gamma = \beta$, the macroscopic foliation angle (Figures 1 and 9), corresponding to a "plane of weakness" [*Jaeger and Cook*, 1979; *Walsh and Brace*, 1964]. For this anisotropic scenario, one expects γ to be fixed and unrelated to the friction coefficient μ. We derived the condition for wing crack nucleation for this case on the basis of *Cotterell and Rice*'s [1980] analysis. The mathematical details are presented in Appendix A. This "anisotropic nucleation" condition is also linear like equation (1), but with a different slope and intercept:

$$m = \frac{\sin 2\beta + \mu(1+\cos 2\beta)}{\sin 2\beta - \mu(1-\cos 2\beta)}, \tag{3a}$$

and

$$c = \frac{\sqrt{3}}{\sin 2\beta - \mu(1-\cos 2\beta)}\frac{K_{1C}}{\sqrt{\pi a}}. \tag{3b}$$

Unlike the isotropic case, for which the slope m and intercept c depend only on the friction coefficient μ and

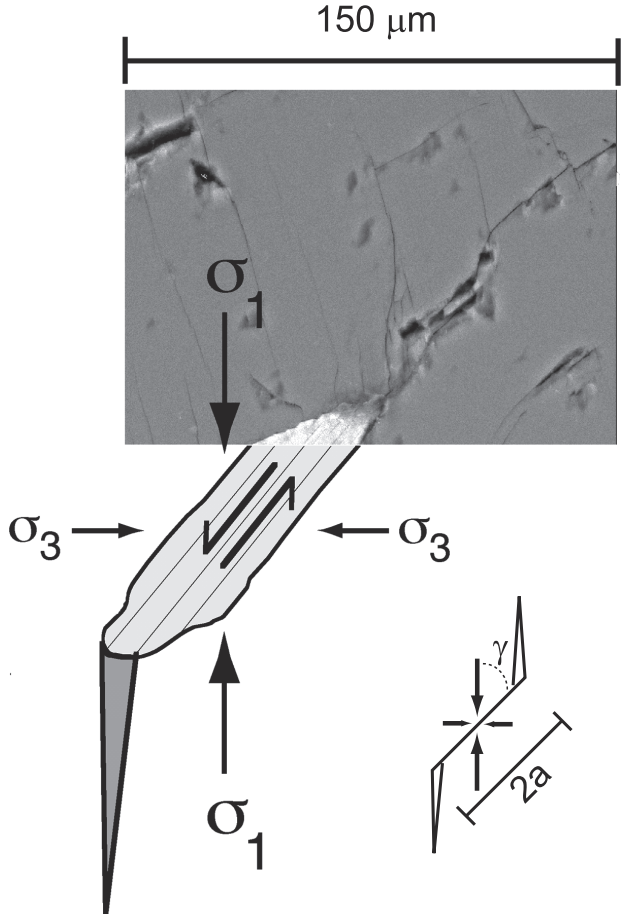

Figure 9. Schematic diagram of a wing crack nucleated from a sliding crack. Geometric parameters of the model are also defined.

Table 2. Parameters Inferred From Damage Mechanics Model

Foliation Angle β	Friction Coefficient μ[a]	Initial Damage D_o	Normalized Fracture Toughness $K_{1C}/\sqrt{\pi a}$, MPa
0°	(0.38)	0.082	93
30°	0.26 (0.28)	0.095	80
45°	0.24 (0.23)	0.110	95
60°	0.22 (0.30)	0.093	90
90°	(0.39)	0.088	88

[a] Values with and without brackets were derived using the isotropic and anisotropic nucleation conditions, respectively.

toughness parameter $K_{1C}/\sqrt{\pi a}$, the parameters in the anisotropic case depend also on the foliation angle β. Note also that equations (3a) and (3b) should only be applied to intermediate foliation orientations, because they predict physically unrealistic stress states for both $\beta = 0$ and $\beta > \tan^{-1}(1/\mu)$.

[33] If we identify macroscopic dilatancy with the nucleation of wing cracks, then the onset of dilatancy C' should correspond to the critical stress state given by equation (1). Since the stresses follow linear trends, the slope and intercept can be determined by linear regression. From the slope m, we can use either equation (2a) or (3a) to infer the coefficient μ for frictional sliding on the inclined crack surface. Values inferred from the isotropic model are compiled in Table 2 and are shown as dark circles in Figure 10. For comparison, values for the relatively isotropic Westerly granite and San Marcos gabbro are also shown.

[34] Our microstructural observations suggest that the anisotropic nucleation model is more appropriate for samples with intermediate foliation angles ($\beta = 30°$, 45°, and 60°). As discussed above, for orientations $\beta = 0°$ and 90° biotite is not oriented favorably for slip and typically deforms by kinking and faulting, respectively. As shown in Figure 10, μ values (light circles) inferred from equation (3a) are somewhat lower than those calculated from the isotropic model and vary over a smaller range (Table 2). For all angles, the inferred values for the Four-mile gneiss (with 9% biotite) are lower than that of Westerly granite (with 5% biotite). For the intermediate angles, our inferred μ values are comparable to that of San Marcos gabbro (with 12% biotite) and within the range (0.26–0.31) determined for frictional sliding on cleavage surfaces of biotite [*Horn and Deere*, 1962]. Relatively low friction on mica cleavages allows dilatancy to initiate at somewhat lower stresses.

[35] Using μ values so inferred we can next use equation (2b) or (3b) to infer from the intercept c the parameter $K_{1C}/\sqrt{\pi a}$. Alternatively we can use the brittle strength data to infer the fracture mechanics parameter. Since recent studies of *Baud et al.* [2000a, 2000b] have shown that this latter approach is more robust, we have adopted their methodology for the inference of the fracture mechanics parameters, to be discussed in the next section.

4.2. Critical Condition for Crack Coalescence and Brittle Failure

[36] A number of damage mechanics models [e.g., *Horii and Nemat-Nasser*, 1986; *Kemeny and Cook*, 1987; *Ashby and Sammis*, 1990] have been formulated to describe the propagation and coalescence of wing cracks. Specific differences among the various micromechanical models were reviewed by *Fredrich et al.* [1990] and *Kemeny and Cook* [1991], but their predictions are qualitatively similar. After initial nucleation, wing cracks propagate stably along a trajectory subparallel to σ_1. The stable growth of a multiplicity of wing cracks results in progressive development of dilatancy. When the stress-induced cracks achieve a critical geometry, crack coalescence and shear localization occur. The critical stress state at which this instability occurs is sensitively dependent on the preexisting damage, characterized by abundance of potential sliding crack surfaces and the size distribution.

[37] For mathematical convenience we have adopted *Ashby and Sammis'* [1990] 2-dimensional damage mechanics model to analyze the development of brittle failure and the influence of mica content and foliation orientation on brittle strength. The key damage parameter in this model is the crack density $D = \pi(\ell + a\cos\gamma)^2 N_A$, where ℓ is the length of the wing crack, and N_A is the number of sliding cracks per unit area initially present. Before wing cracks nucleate, the length $\ell = 0$ and therefore the initial damage is given by $D_o = \pi(a\cos\gamma)^2 N_A$. With the progressive development of dilatancy, the principal stresses evolve with damage in accordance with equation (17) of *Ashby and Sammis* [1990]:

$$\sigma_1 = \left[C_1 + \frac{C_4\left(\sqrt{D/D_o} - 1\right)}{1 + \sqrt{\pi D_o}\,\dfrac{\sqrt{D/D_o} - 1}{1 - \sqrt{D}}} \right] \cdot \sigma_3 + \frac{\left(\sqrt{D/D_o} - 1 + 0.1/\cos\gamma\right)^{1/2}}{1 + \sqrt{\pi D_o}\,\dfrac{\sqrt{D/D_o} - 1}{1 - \sqrt{D}}} \frac{C_4}{\sqrt{\cos\gamma}} \frac{K_{1C}}{\sqrt{\pi a}} \qquad (4)$$

where $C_1 = (\sqrt{1+\mu^2} + \mu)/(\sqrt{1+\mu^2} - \mu)$ and $C_4 = \sqrt{30}\cos\gamma/(\sqrt{1+\mu^2} - \mu)$. Although microcracks may be nucleated from

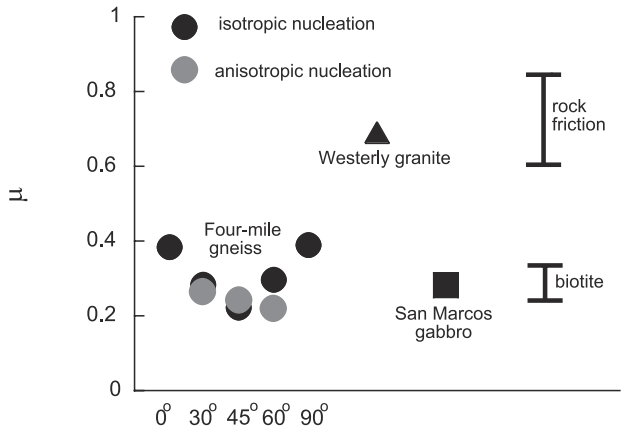

Figure 10. Friction coefficient as a function of foliation angle β inferred from dilatancy onset data on the basis of the wing crack model using isotropic and anisotropic nucleation conditions. Friction coefficients for Westerly granite (from data of *Brace et al.* [1966]) and San Marcos gabbro (from data of *Hadley* [1973]) were calculated using the isotropic nucleation model. For comparison, experimental values for rock friction [*Byerlee*, 1978] and biotite friction [*Horn and Deere*, 1962] are shown.

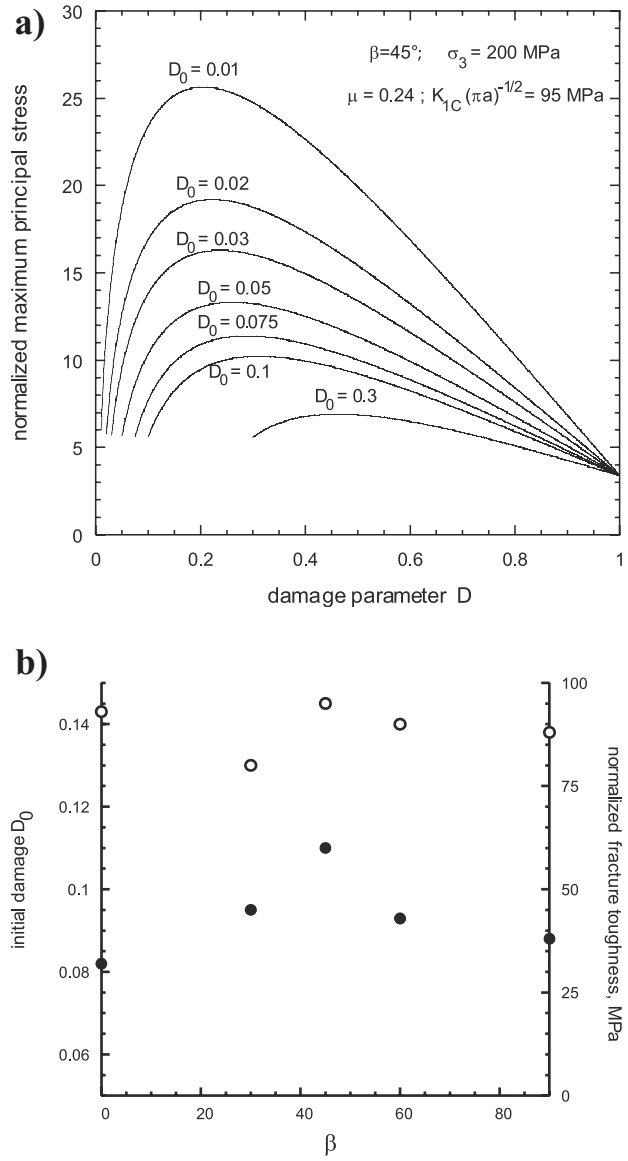

Figure 11. (a) Normalized principal stress $\sigma_1\sqrt{\pi a}/K_{1C}$ as a function of accumulated damage for various initial damage D_o. The parameters used for the damage mechanics model are as indicated. (b) Inferred values of initial damage (solid circles) and normalized fracture toughness $K_{1C}/\sqrt{\pi a}$ (open circles) as functions of foliation angle of the Four-mile gneiss.

sliding cracks of specific orientations, the ultimate failure and instability arise from the interaction and coalescence of numerous microcracks nucleated from sliding cracks with a range of γ values. It is implicitly assumed in the derivation of the above equation that the cooperative effects of the multiplicity of cracks are approximated by choosing an "effective" value of $\gamma = 45°$.

[38] If one specifies the material parameters D_o, $K_{IC}/\sqrt{\pi a}$ and μ, then the evolution of the principal stress σ_1 as a function of damage D at a fixed confining stress σ_3 can be calculated using equation (4). In the brittle regime, the damage accumulation is manifested first by strain hardening and then by strain softening (Figure 11a). The critical stress state at which instability occurs is identified as the peak value at the transition from hardening to softening for each curve.

[39] Repeating the calculation for different values of fixed σ_3 allows one to map out the brittle failure envelope in the principal stress space. To a first approximation this failure envelope for the wing crack model [*Horii and Nemat-Nasser*, 1986; *Ashby and Sammis*, 1990; *Fredrich et al.*, 1990; *Kemeny and Cook*, 1991; *Baud et al.*, 2000a, 2000b] can be described by a linear relation

$$\sigma_1 = A(\mu, D_o)\sigma_3 + B(\mu, D_o)K_{IC}/\sqrt{\pi a} \qquad (5)$$

If triaxial compression data for the onset of dilatancy and peak stress follow the linear trends described by equations (1) and (5), then the slopes and intercepts of the two sets of stress data provide four constraints for inferring the three parameters D_o, $K_{IC}/\sqrt{\pi a}$, and μ. As discussed above, we have used the onset of dilatancy data and equation (1) to constrain μ, and the peak stress data and equation (5) to constrain D_o and $K_{IC}/\sqrt{\pi a}$. The parameters so inferred are compiled in Table 2.

[40] The inferred values of $K_{IC}/\sqrt{\pi a}$ fall in a relatively narrow range (of 80–95 MPa) and do not show any systematic trends with foliation (Table 2). This suggests that even though there are significant differences in friction coefficients for sliding on mica cleavages (for the intermediate range of β) and for sliding on cracks embedded in other minerals (for very low and high values of β), ultimate failure involves numerous cracks that propagate in different minerals and the inferred values of $K_{IC}/\sqrt{\pi a}$ represent an average that is approximately the same for all foliation angles. If we make the plausible assumption [*Fredrich et al.*, 1990] that the sliding crack length $2a$ can be approximated by the average grain size, then the fracture toughness can be inferred. For example, if $a \sim 1$ mm, then K_{IC} is inferred to range from 4.5 to 5.3 MPa $m^{1/2}$, comparable to the high end of experimental values for silicate rocks [*Atkinson and Meredith*, 1987].

[41] The range of D_o (Table 2) is comparable to the values given by *Ashby and Sammis* [1990] for granite, eclogite, dunite, and gabbro. There is a trend for the initial damage to be higher in the intermediate range of foliation angles (Figure 11b), indicating a negative correlation with the peak stress (Figure 4b). The reduction of brittle strength in the intermediate range of foliation angles can therefore be attributed to an enhancement of initial damage as well as reduction of friction coefficient along the mica cleavages. We interpret the initial damage to be from two contributions: a set of preexisting microcracks with random orientation, and a set of cleavage cracks in mica grains preferentially oriented along the foliation angle. The minimum D_o values of $\beta = 0°$ and 90° correspond to the first set, with negligible contribution from mica cleavages. The enhanced D_o values for intermediate β angles arise from the additional contributions from the favorably oriented mica cleavages.

4.3. Influence of Damage State and Mica Content on the Brittle Strength

[42] The damage mechanics model predicts that the brittle strength decreases with increasing initial damage D_o (Figure 11a), and we interpret the initial damage to

Table 3. Strengths of Foliated Rocks With Different Mica Contents

Experiment Number[a]	Formation Name	Peak Stress, MPa	Failure Mode	Mica Content f_m	Inferred Initial Damage D_o
FMG15	Four-mile	737	brittle	0.10	0.110
R81	Four-mile	787	brittle	0.10	0.096
R28	Four-mile	513	brittle	0.10	0.236
A2-14301	DH2-43.6m	464	brittle	0.16	0.290
A4-559-01	DH4-170.4m	488	brittle	0.21	0.264
A4-248-01	DH4-74.6m	206	transitional	0.25	[b]
A2-416-01S	DH2-126.8m	260	brittle	0.27	[b]
A4-793-01	DH4-241.8m	366	transitional	0.33	0.482
BG S01	Rough Ridge	403	transitional	0.37	0.390
MS S01	Honey I	353	transitional	0.46	0.525

[a] The experimental data are from *Shea and Kronenberg* [1993], except for FMG15 (from this study) and R81 and R28 [from *Gottschalk et al.*, 1990].

[b] These two samples had anomalously low strengths and were not used in the linear regression for equation (6). Sample DH2-126.8m has relatively high calcite content of ~3%.

include an important contribution from cleavage cracks in mica grains. It has also been observed that the strength of a foliated rock decreases with increasing mica content f_m [*Shea and Kronenberg*, 1993]. These observations therefore suggest that the damage and mica content are correlated.

[43] Experimental data for the strength of eight gneisses as a function of mica content f_m (for $\beta = 45°$ and $P_c = 200$ MPa) from *Shea and Kronenberg* [1993] and this study are compiled in Table 3 and Figure 12a. *Shea and Kronenberg*'s [1993] data are for samples with 10 to 46% mica that failed in a brittle or semibrittle manner. For each gneiss sample, we can use the damage mechanics model (with $\mu = 0.24$ and $K_{IC}/\sqrt{\pi a} = 95$ MPa, values appropriate for the Four-mile gneiss with $\beta = 45°$) to calculate the D_o value that corresponds to the experimentally determined strength for $\sigma_3 = 200$ MPa. As shown in Figure 12b, there is an approximately linear correlation between mica content f_m and initial damage D_o so calculated, except for two samples (marked in Table 3) that had anomalously low strengths. *Shea and Kronenberg* [1993] reported that one of the samples had 3% calcite, which suggests that it may have been altered, perhaps along macroscopic fractures. A linear regression excluding these two points results in the following relation between mica content and initial damage D_o:

$$D_o = D_o^m f_m + D_o^c \quad (6)$$

with $D_o^m = 1.04$ and $D_o^c = 0.06$. In light of our microstructural observations that preexisting damage is usually associated with cleavage planes in mica acting as sliding cracks, the correlation between D_o and f_m is reasonable. In fact, if we assume that the damage state in each mica grain in all of the gneisses is about the same, then D_o^m can be interpreted as an "intrinsic" damage parameter that is relatively constant in all of the grains, whereas D_o^c is damage unrelated to mica content, representing a population of randomly oriented cracks in the other minerals or grain boundary cracks. It is of interest to note that this estimate of D_o^c is comparable to the minimum values of D_o (0.08 and 0.09) inferred for $\beta = 0°$ and 90°, which we have attributed to the same set of preexisting microcracks with random orientation.

[44] It must be noted that the above analysis assumes that the other gneisses have values of $K_{IC}/\sqrt{\pi a}$ that are identical to what we inferred from the strength data of the Four-mile gneiss. Because all of the rocks are quartzo-feldspathic gneisses, it is plausible that K_{IC} does not vary significantly among them. However, it is difficult to estimate the sliding crack length a since for each rock there is a range of biotite grain sizes. The damage parameter D_o itself is difficult to characterize quantitatively because it depends on details of the crack statistics [*Wong*, 1985]. However, it can be specified for a certain idealized geometry. In a 2-dimensional model, if we consider mica grains with uniform length L and width W and if there are n cleavage cracks in each grain, then the number of cracks per unit area is $N_A = nf_m/(LW)$. If each cleavage crack extends across the grain, then its length is $2a = L$, and therefore the initial damage is given by $D_o = (\pi/2)N_A a^2 = (\pi/8)(L/W)\, nf_m$ and $n = (8/\pi)(W/L)D_o^m$. As an example, if the average aspect ratio of mica

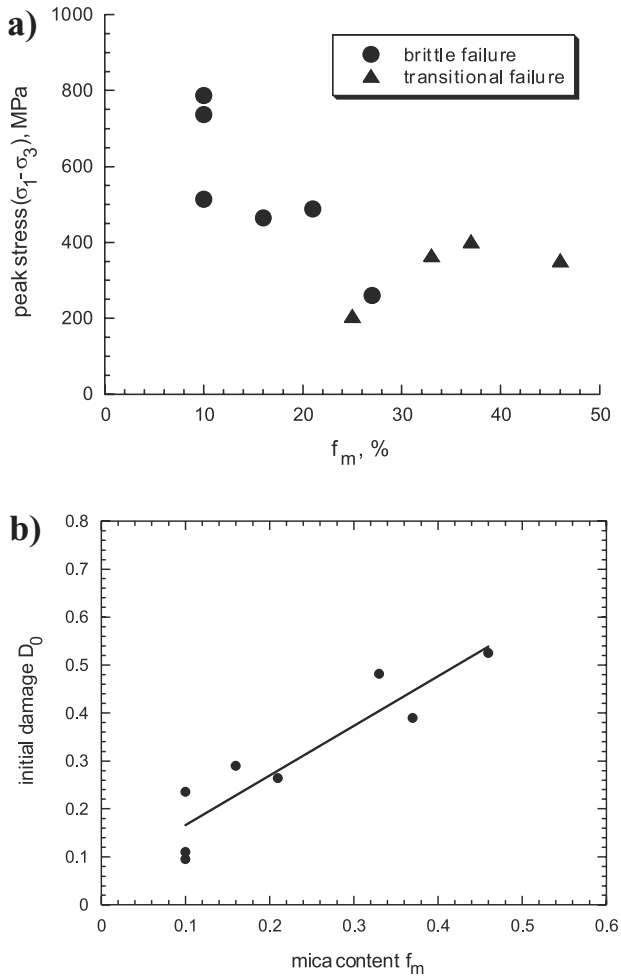

Figure 12. (a) Strength of foliation rock as a function of mica content. These data are also compiled in Table 3. (b) Inferred value of initial damage as a function of mica content. Two data points have been excluded as noted in Table 3. The line from linear regression is also shown.

grain is $L/W \sim 5$, then our inferred value of $D_o^m = 1.04$ corresponds to $n \sim 0.5$ cracks per grain.

5. Discussion

[45] Our mechanical data for the Four-mile gneiss show that the foliation angle exerts significant control over the onset of dilatancy and brittle fracture. There is positive correlation between dilatancy and strength anisotropies. If indeed this correlation between dilatancy and strength anisotropies is representative of foliated rocks, it will have several tectonic implications. Recent studies [*Vernik and Zoback*, 1990; *Vernik et al.*, 1992a, 1992b] have addressed the considerable effect of mechanical anisotropy in the surrounding rock on the morphology and interpretation of wellbore breakout and inference of in situ stress. *Vernik et al.* [1992b] showed that breakout morphology and occurrence are influenced by anisotropic rock strength and an effective pressure drop around the borehole due to infiltration of drilling fluid into the wall rock. Implicit in their interpretation of breakout data is the anisotropy of the dilatancy stress C', at which point fluid infiltration begins. Our data provide the mechanical basis for this assumption on the correlation between dilatancy and strength anisotropy.

[46] Numerous natural examples of fluid flow and associated alteration around dilatant cracks have been described in the literature, and it is of interest to speculate on the potential influence of dilatancy anisotropy. *Segall and Pollard* [1983] documented the nucleation of small faults on preexisting dilatant fractures in granite and associated local retrograde alteration of the host rock through fluid infiltration. *Simpson* [1986], *Segall and Simpson* [1986], and *Gibson* [1990] described much more intense retrograde metamorphism and reaction softening that led to ductile shear zone formation in rocks that initially deformed in a brittle manner. *McCaig* [1987] emphasized the large volume of fluid involved and the interplay of deformation and mineral reactions. The relative orientations of the host rock foliation and shear zone or phyllonite foliation in several of *Gibson*'s [1990] thin section photos (his Figures 3c, 6d, 6e, and 7a) are suggestive of the deformation microstructure we observed in the Four-mile gneiss. *Gibson* [1990] argued that initial brittle cracking and eventual ductile shear zone formation occurred under the same stress regime. Assuming that strain rates are low enough and permeability or fluid pressures are high enough [*Etheridge et al.*, 1984] to allow rapid fluid infiltration, the onset of reaction softening may be sensitively dependent on onset of dilatancy C'. Thus on geologic scales of tens of meters or more, anisotropy of C' with foliation orientation relative to the far-field principal stresses should strongly affect the spatial localization of strain. Thus, analogous to the mechanism of borehole breakout discussed above, in the presence of fluids, anisotropy of dilatancy may be more significant in controlling deformation than brittle strength anisotropy.

[47] While our damage mechanics model seems to capture most of the first-order observations on dilatancy and brittle failure in the gneiss, there are a few limitations that should be noted. First, even though the mechanical and microstructural data indicate that an anisotropic nucleation condition should be adopted for the intermediate foliation angles, the theory does not specify at what range of foliation angles such a condition is more appropriate. To address this question, data for samples with a finer division of foliation angles would be required to guide the development of a more elaborate micromechanical model. Second, an intrinsic limitation of the wing crack type of model is that failure occurs as an instability in crack growth without specific prediction of the angle of macroscopic failure. Therefore the damage mechanics model cannot address the question as to why the macroscopic failure angle for the Four-mile gneiss is $\sim 30°$, seemingly independent of the foliation angle. *Gottschalk et al.* [1990] compiled their fracture angle data for this rock which do not show any systematic correlation with the foliation angles. In contrast, correlation of failure mode and foliation angle was documented in a strongly foliated slate [*Donath*, 1964]. To elucidate the micromechanics responsible for this apparent discrepancy in the failure modes of different types of foliated rock, further systematic study is warranted. Third, our analysis is based on a 2-dimensional wing crack model. Recent 3-dimensional results of *Germanovich et al.* [1994] have underscored a number of differences that arise from geometric complexity, which should be consider in future theoretical analysis of damage development in a foliated rock.

6. Conclusion

[48] Significant anisotropies are associated with the development of dilatancy and brittle failure in the Four-mile gneiss. Both the onset of dilatancy and ultimate strength attain minimum values at intermediate foliation angles. Our microstructural observations underscore the important role played by the preferentially oriented mica grains in the development of dilatancy. The preferred orientation of biotite in the Four-mile gneiss results in anisotropies of the dilatancy onset and peak stresses which become greater with increasing confining pressure. The onset of dilatancy at intermediate foliation orientations is due to tensile microcracks nucleated by frictional slip on biotite. Kinking and elastic mismatch cracking are important deformation processes when the foliation is parallel and perpendicular, respectively, to the compression axis.

[49] The sliding wing crack model provides an explanation for the dilatancy anisotropy as a function of foliation orientation. Using the anisotropic nucleation condition for the intermediate foliation angles, frictional coefficients for the sliding cracks are inferred to be comparable to cleavage surfaces of biotite. Relatively low friction on mica cleavages allows dilatancy to initiate at somewhat lower stresses for the onset of dilatancy.

[50] The strength anisotropy data of the Four-mile gneiss can be explained by the damage mechanics model, with the assumption that the initial damage varies with the foliation angle. The initial damage is inferred to be higher for the intermediate angles, which is plausible if the damage derives from two contributions: a set of preexisting microcracks with random orientation, and a set of cleavage cracks in mica grains preferentially oriented along the foliation angle. The observation that the mechanical strength (for foliated rocks at $\beta = 45°$) decreases with increasing mica content can also be explained by the damage mechanics model, with the assumption that the initial damage and mica

content are linearly related. When the mica content is negligible, then the initial damage is due to a population of randomly oriented cracks in the other minerals or grain boundary cracks, with a value comparable to those for foliation angles $\beta = 0°$ or 90°.

Appendix A: Derivation of the Microcrack Nucleation Conditions

[51] To establish the critical condition for the growth of a wing crack, we need to first calculate the stress intensity factor of a putative crack that nucleates from the tip of the main sliding crack. The loading configuration and geometric notation are as illustrated in Figure 9. The resolved shear stress and normal stress that act on the main sliding crack are given by $\tau = (\sigma_1 - \sigma_3)/2 \sin 2\gamma$ and $\sigma_n = (\sigma_1 + \sigma_3)/2 - (\sigma_1 - \sigma_3)/2 \cos 2\gamma$, respectively. Since the frictional coefficient is μ, frictional slip may occur if the shear stress is sufficiently large and the "effective" shear stress acting on the sliding crack surface is then given by

$$\tau^* = \tau - \mu\sigma_n = \frac{\sigma_1 - \sigma_3}{2}\sin\ 2\gamma - \mu\left(\frac{\sigma_1 + \sigma_3}{2} - \frac{\sigma_1 - \sigma_3}{2}\cos\ 2\gamma\right). \tag{A1}$$

Up to this point we have consistently followed the convention that compressive stress is positive. However, it is more appropriate to adopt the other convention (that tensile stress is positive) when one analyzes the stress intensity factors, especially since we will use results derived by *Cotterell and Rice* [1980] who also followed this convention. Accordingly the mode-II stress intensity factor associated with the sliding crack (of length $2a$) is given by

$$k_{II} = -\tau^*\sqrt{\pi a}, \tag{A2}$$

whereas the mode-I factor $k_I = 0$ since the sliding crack is closed.

[52] In their equation (31) *Cotterell and Rice* [1980] presented an asymptotic solution for the mode-I and -II stress intensity factors at the tip of a wing crack (of infinitesimal length at an angle θ to the sliding crack)

$$\begin{aligned} K_I &= C_{11}k_I + C_{12}k_{II} \\ K_{II} &= C_{21}k_I + C_{22}k_{II}, \end{aligned} \tag{A3}$$

where the coefficients C_{ij} are functions of θ and in particular $C_{12} = -3/4(\sin(\theta/2) + \sin(3\theta/2))$. The extensile wing crack nucleates at the angle θ that maximizes the stress intensity factor

$$K_I = C_{12}k_{II} = \frac{3}{4}\tau^*\sqrt{\pi a}\left(\sin\frac{\theta}{2} + \sin\frac{3\theta}{2}\right). \tag{A4}$$

By differentiating the above expression with respect to θ and setting the derivative to 0, one concludes that the preferred angle satisfies $\cos\theta = 1/3$ and equals 70.5°. Substituting this θ value into equation (A4) and imposing the crack propagation criterion $K_I = K_{IC}$ we arrive at

$$K_I = \frac{2}{\sqrt{3}}\tau^*\sqrt{\pi a} = K_{IC}. \tag{A5}$$

Substituting (A1) into (A5) and rearranging the equation, we have

$$\frac{\sigma_1 - \sigma_3}{2}\sin\ 2\gamma - \mu\left(\frac{\sigma_1 + \sigma_3}{2} - \frac{\sigma_1 - \sigma_3}{2}\cos\ 2\gamma\right) = \frac{\sqrt{3}}{2}\frac{K_{IC}}{\sqrt{\pi a}}. \tag{A6}$$

[53] For our anisotropic nucleation condition, the sliding cracks are assumed to be preferentially aligned along the foliation direction and hence $\gamma = \beta$, which when substituted into equation (A6) gives the linear relation (1) between the principal stresses with slope and intercept given by (3a) and (3b), respectively. For the isotropic nucleation condition the sliding cracks are assumed to be randomly distributed and hence we seek the angle γ that maximizes the effective shear stress τ^* given by (A1). This critical angle is given by $\gamma = 1/2\ \tan^{-1}(1/\mu)$, which when substituted into equation (A6) gives the linear relation (1) between the principal stresses with slope and intercept given by (2a) and (2b), respectively.

[54] **Acknowledgments.** We are grateful to Peter Robinson of the University of Massachusetts for providing guidance on sample collection, and to Andreas Kronenberg of Texas A&M University for providing us with starting materials. We are grateful to Richard Yund for the use of the ion-milling facilities at Brown University. We have benefited from constructive comments of the associate editor Ian Main and reviewers Leonid Germanovich and Bazalel Haimson. Discussions with Joanne Fredrich, Emmanuelle Klein, Andreas Kronenberg and Veronika Vajdova have also been very helpful. This research was partially supported by the Office of Basic Energy Sciences, Department of Energy under grant DEFG0299ER14996.

References

Amadei, B., *Rock Anisotropy and the Theory of Stress Measurements*, 478 pp., Springer-Verlag, New York, 1983.

Ashby, M. F., and S. D. Hallam, The failure of brittle solids containing small cracks under compressive stress states, *Acta Metall.*, *34*, 497–510, 1986.

Ashby, M. F., and C. G. Sammis, The damage mechanics of brittle solids in compression, *Pure Appl. Geophys.*, *133*, 489–521, 1990.

Atkinson, B. K., and P. G. Meredith, Experimental fracture mechanics data for rocks and minerals, in *Fracture Mechanics of Rock*, edited by B. K. Atkinson, pp. 477–525, Academic, San Diego, Calif., 1987.

Barroul, G., and D. Mainprice, A quantitative evaluation of the contribution of crustal rocks to the shear-wave splitting of teleseismic SKS waves, *Phys. Earth Planet. Inter.*, *78*, 281–300, 1993.

Baud, P., A. Schubnel, and T.-f. Wong, Dilatancy, compaction and failure mode in Solnhofen limestone, *J. Geophys. Res.*, *105*, 19,289–19,303, 2000a.

Baud, P., W. Zhu, and T.-f. Wong, Failure mode and weakening effect of water on sandstone, *J. Geophys. Res.*, *105*, 16,371–16,390, 2000b.

Borg, I., and J. Handin, Experimental deformation of crystalline rocks, *Tectonophysics*, *3*, 249–368, 1966.

Brace, W. F., Some new measurements of linear compressibility of rocks, *J. Geophys. Res.*, *70*, 391–398, 1965.

Brace, W. F., and E. G. Bombolakis, A note on brittle crack growth in compression, *J. Geophys. Res.*, *68*, 3709–3713, 1963.

Brace, W. F., B. Paulding, and C. H. Scholz, Dilatancy in the fracture of crystalline rocks, *J. Geophys. Res.*, *71*, 3939–3954, 1966.

Byerlee, J. D., Friction of rocks, *Pure Appl. Geophys.*, *116*, 615–626, 1978.

Chang, C., and B. Haimson, True triaxial strength and deformability of the German Continental Deep Drilling Program (KTB) deep hole amphibolite, *J. Geophys. Res.*, *105*, 18,999–19,013, 2000.

Cotterell, B., and J. R. Rice, Slightly curved or kinked cracks, *Int. J. Fract.*, *16*, 155–169, 1980.

Donath, F. A., Strength variation and deformational behaviour in anisotropic rock, in *State of Stress in the Earth's Crust*, edited by W. R. Judd, pp. 281–297, Elsevier Sci., New York, 1964.

Donath, F. A., Effects of cohesion and granularity on deformational behavior of anisotropic rock, in *Studies in Mineralogy and Precambrian Geology*, *Geol. Soc. Am. 135*, edited by B. R. Doe and D. K. Smith, pp. 95–128, Boulder, Colo., 1972.

Etheridge, M. A., V. J. Wall, S. F. Cox, and R. H. Vernon, High fluid pressures during regional metamorphism and deformation: Implications for mass transport and deformation mechanisms, *J. Geophys. Res.*, *89*, 4344–4358, 1984.

Fredrich, J., B. Evans, and T.-f. Wong, Effects of grain size on brittle and semi-brittle strength: Implications for micromechanical modelling of failure in compression, *J. Geophys. Res.*, *95*, 10,729–11,358, 1990.

Fredrich, J. T., B. Evans, and T.-f. Wong, Micromechanics of the brittle to plastic transition in Carrara marble, *J. Geophys. Res.*, *94*, 4129–4145, 1989.

Gay, N. C., and L. E. Weiss, The relationship between principal stress directions and the geometry of kinks in foliated rocks, *Tectonophysics*, *21*, 287–300, 1974.

Germanovich, L. N., R. L. Salganik, A. V. Dyskin, and K. K. Lee, Mechanisms of brittle fracture of rock with pre-existing cracks in compression, *Pure Appl. Geophys.*, *143*, 117–149, 1994.

Gibson, R. G., Nucleation and growth of retrograde shear zones: An example from the Needle Mountains, Colorado, U.S.A., *J. Struct. Geol.*, *12*, 339–350, 1990.

Gottschalk, R. R., A. K. Kronenberg, J. E. Russell, and J. Handin, Mechanical anisotropy of gneiss: Failure criterion and textural sources of directional behavior, *J. Geophys. Res.*, *95*, 21,613–21,634, 1990.

Hadley, K., Laboratory investigation of dilatancy and motion on fault surfaces at low confining pressures, in *Proceedings of the Conference on Tectonic Problems of the San Andreas Fault System*, edited by R. L. Kovach and A. Nur, pp. 427–435, Stanford Univ., Stanford, Calif., 1973.

Hirth, G., and J. Tullis, The effects of pressure and porosity on the micromechanics of the brittle-ductile transition, *J. Geophys. Res.*, *94*, 17,825–17,838, 1989.

Horii, H., and S. Nemat-Nasser, Brittle failure in compression: Splitting, faulting and brittle-ductile transition, *Philos. Trans. R. Soc. London*, *319*, 337–374, 1986.

Horn, H. M., and D. U. Deere, Frictional characteristics of minerals, *Geotechnique*, *12*, 319–335, 1962.

Jaeger, J. C., Shear failure of anisotropic rocks, *Geol. Mag.*, *97*, 65–72, 1960.

Jaeger, J. C., and N. G. W. Cook, *Fundamentals of Rock Mechanics*, 3rd ed., 593 pp., Chapman and Hall, New York, 1979.

Kemeny, J. M., and N. G. W. Cook, Crack models for the failure of rocks in compression, *Proc. Int. Conf. Const. Laws Eng. Mater.*, *2*, 879–887, 1987.

Kemeny, J. M., and N. G. W. Cook, Micromechanics of deformation in rocks, in *Toughening Mechanisms in Quasi-Brittle Materials*, edited by S. P. Shah, pp. 155–188, Kluwer Acad, Norwell, Mass., 1991.

Kranz, R. L., Crack growth and development during creep in Westerly granite, *Int. J. Rock Mech. Min. Sci.*, *16*, 23–36, 1979.

Kranz, R. L., Microcracks in rocks, a review, *Tectonophysics*, *100*, 449–480, 1983.

Kronenberg, A. K., S. H. Kirby, and J. Pinkston, Basal slip and mechanical anisotropy of biotite, *J. Geophys. Res.*, *95*, 19,257–19,278, 1990.

Liao, J. J., M.-T. Yang, and H.-Y. Hsieh, Direct tensile behavior of a transversely isotropic rock, *Int. J. Rock Mech. Min. Sci.*, *34*, 837–849, 1997.

McCaig, A. M., Deformation and fluid–rock interaction in metasomatic dilatant shear bands, *Tectonophysics*, *135*, 121–132, 1987.

McLamore, R., and K. E. Gray, The mechanical behaviour of anisotropic sedimentary rocks, *Trans. Am. Soc. Mech. Eng. Ser. B*, *89*, 62–73, 1967.

Niandou, H., J. F. Shao, J. P. Henry, and D. Fourmaintraux, Laboratory investigation of the mechanical behavior of Tournemire shale, *Int. J. Rock. Mech. Min. Sci.*, *34*, 3–16, 1997.

Nova, R., and A. Zaninetti, An investigation into the tensile behavior of a schistose rock, *Int. J. Rock Mech. Min. Sci.*, *27*, 231–242, 1990.

Paterson, M. S., *Experimental Rock Deformation—The Brittle Field*, 254 pp., Spinger-Verlag, New York, 1978.

Paterson, M. S., and L. E. Weiss, Experimental deformation and folding in phyllite, *Geol. Soc. Am. Bull.*, *77*, 343–374, 1966.

Sammis, C. G., and M. F. Ashby, The failure of brittle porous solids under compressive stress states, *Acta Metall.*, *34*, 511–526, 1986.

Segall, P., and D. D. Pollard, Nucleation and growth of strike-slip faults in granite, *J. Geophys. Res.*, *88*, 555–568, 1983.

Segall, P., and C. Simpson, Nucleation of ductile shear zones on dilatant fractures, *Geology*, *14*, 56–59, 1986.

Shea, W. T., and A. K. Kronenberg, Strength and anisotropy of foliated rocks with varied mica contents, *J. Struct. Geol.*, *15*, 1097–1121, 1993.

Siegesmund, S., A. Vollbrecht, T. Chlupac, G. Nover, H. Durrast, J. Muller, and K. Weber, Fabric-controlled anisotropy of petrophysical properties observed in KTB core samples, *Sci. Drill.*, *4*, 31–54, 1993.

Simmons, G., and H. F. Wang, *Single Crystal Elastic Constants and Calculated Aggregate Properties: A Handbook*, 370 pp., MIT Press, Cambridge, Mass., 1971.

Simpson, C., Fabric development in brittle-to-ductile shear zones, *Pure Appl. Geophys.*, *124*, 269–288, 1986.

Tapponier, P., and W. F. Brace, Development of stress-induced microcracks in Westerly granite, *Int. J. Rock Mech. Min. Sci.*, *13*, 103–112, 1976.

Tien, Y. M., and P. F. Tsao, Preparation and mechanical properties of artificial transversely isotropic rock, *Int. J. Rock Mech. Min. Sci.*, *37*, 1001–1012, 2000.

Vernik, L., and M. D. Zoback, Strength anisotropy in crystalline rock: Implications for assessment of in situ stresses from wellbore breakouts, in *Rock Mechanics Contributions and Challenges*, edited by W. A. Hustrulid and G. A. Johnson, pp. 841–848, Balkema, Rotterdam, 1990.

Vernik, L., D. Lockner, and M. D. Zoback, Anisotropic strength of some typical metamorphic rocks from the KTB pilot hole, Germany, *Sci. Drill.*, *3*, 153–160, 1992a.

Vernik, L., M. D. Zoback, and M. Brudy, Methodology and application of the wellbore breakout analysis in estimating the maximum horizontal stress magnitude in the KTB pilot hole, *Sci. Drill.*, *3*, 161–169, 1992b.

Walsh, J. B., and W. F. Brace, A fracture criterion for brittle anisotropic rock, *J. Geophys. Res.*, *69*, 3449–3456, 1964.

Wong, T.-f., Micromechanics of faulting in Westerly granite, *Int. J. Rock Mech. Min. Sci.*, *19*, 49–64, 1982.

Wong, T.-f., Geometric probability approach to the characterization and analysis of microcracking in rocks, *Mech. Mater.*, *4*, 261–276, 1985.

Wong, T.-f., and R. Biegel, Effects of pressure on the micromechanics of faulting in San Marcos gabbro, *J. Struct. Geol.*, *7*, 737–749, 1985.

Wong, T.-f., C. David, and W. Zhu, The transition from brittle faulting to cataclastic flow in porous sandstones: Mechanical deformation, *J. Geophys. Res.*, *102*, 3009–3025, 1997.

P. Baud, Institut de Physique du Globe, Université de Louis Pasteur, Strasbourg, France.

G. C. Rawling, New Mexico Bureau of Geology and Mineral Resources, Socorro, NM, USA.

T.-f. Wong, Department of Geosciences, State University of New York at Stony Brook, ESS Building, Stony Brook, NY 11794-2100, USA. (Teng-fong.Wong@sunysb.edu)